Josep Maria Cantons Pérez

LABEL-FREE SENSOR FOR THE NEAR REAL-TIME DETECTION OF PROSTATE CANCER

MASTER'S DEGREE THESIS

Supervised by Dr. Lluis F. Marsal and Dr. Akash Bachhuka

MASTER'S DEGREE IN NANOSCIENCE, MATERIALS AND PROCESSES

UNIVERSITAT ROVIRA I VIRGILI

Tarragona

2022

Label-free sensor for the near real-time detection of prostate cancer

Master in Nanoscience, Materials and Processes, 2021-2022

e-mail: josepmaria.cantons@alumni.urv.cat

Supervisors: Dr. Lluis F. Marsal and Dr. Akash Bachhuka

Department: Department of Electrical, Electronics and Automatic engineering.

Abstract:

Cancer is a disease that occurs when a group of cells in our body start growing in a non-controlled way. There are more than 200 types of cancer, depending on their origin. Among these, prostate cancer was reported to have the most cases in Spain in 2021. To date, the gold standard non-invasive test for the detection of prostate cancer is the prostate-specific antigen (PSA) test which unfortunately has a high false positive rate (75%). Therefore, the current study aimed to fabricate a proof-of-concept (POC) device that can overcome the disadvantages of the current PSA test for the early detection of prostate cancer. To fabricate this POC device, the optical and geometric properties of nanoporous anodic alumina (NAA) were combined with the optical properties of gold nanoclusters (AuNCs). In addition, endoglin (ENG-105) was used as the target protein for the early detection of prostate cancer. The POC device was optimized at various conditions: a) NAA pore size- 35 and 75 nm, b) immobilization of gold nanoclusters- with and without the addition of NHS and EDC, c) the incubation time for both gold nanoclusters and endoglin protein, d) adding different blocking buffers- Ethanolamine and Bovine Serum Albumin (BSA). NAA samples with larger pores (75 nm) showed a higher photoluminescence signal for biomarker detection than NAA samples with small pores (35 nm). Furthermore, the POC device showed sensitivity for the endoglin detection range in fg/ml to ug/ml. However, non-specific binding was observed in the case of the control antibody. Although this study demonstrates the potential of the proposed POC device, further optimization is required to overcome the non-specific binding.

INTRODUCTION

In our body, we have trillions of cells that have different functions. These cells grow, multiplicate, and finally die, completing their life cycle. There are cases in which a group of cells starts growing in an uncontrolled way, which is called cancer. This uncontrolled growth of the cells causes a tumour and spreads to other parts of the body [1]. Due to the complexity of cancer, it is essential to detect it in the early stage as the complexity of cancer increases with time, making it hard to treat the disease. This complexity arises from the alterations induced by cancer in our bodies. These alterations include cell growth in diverse environments invading other tissues and are termed 'metastasis'. This then responds effectively to attacks from the immune system [2].

In the last few decades, the investigation of cancer has increased manifold to look for new diagnosis and treatment tools to detect cancer in its early stages, which is quite essential in the patient's life expectancy. The statistical data from 2021 revealed more than 150.000 cases in the USA from diagnosis of different types of cancer such as breast cancer, lung cancer, prostate cancer, and colon cancer [3]. This work is focused on investigating prostate cancer, as it accounts for a significant number of cases per year. In addition, the obtention of the sample is less complicated. And finally, the non-invasive conventional method for the diagnosis of prostate cancer, called the prostate-specific antigen (PSA) test, shows a high false positive result [4]. Moreover, in Spain, one of the most diagnosed cancers is prostate cancer, with 35.764 cases in 2021 [5].

The main objective of this project is to fabricate a non-invasive point-of-care (POC) device based on a nanoporous alumina membrane to detect biomarkers specific to prostate cancer, which will

aid in its diagnosis and prognosis. These nanoporous membranes will be fabricated from aluminium, previously used in many sensing applications due to its high effective surface area, intrinsic optical properties, and low-cost fabrication [6] [7]. Furthermore, the possibility of altering the optical properties of alumina by changing the fabrication parameters due to its high effective surface area, which is in the order of hundreds of m^2/cm^2, makes it feasible for many sensing applications [8]. There are many applications in which NAA has been used; for example, this material has been used as a material to detect a Salmonella-specific DNA fragment by functionalizing the pore walls. The authors used different concentrations of this bacteria to test the sensor [9]. Another application of nanoporous alumina was for the effective detection of breast cancer. In this study, the porous alumina surface was functionalized to detect micro RNAs, a potential breast cancer biomarker [10]. Apart from the sensing applications, nanoporous alumina is also interesting for drug delivery applications [11] and tissue engineering applications, thanks to its diversity of morphologies [12] [13]. Even though nanoporous alumina has been used in many sensing applications, it has never been used as a sensing material for diagnosing prostate cancer. Therefore, in our current study, we propose to functionalize the surface of these nanoporous membranes with antigen-specific antibodies to capture biomarkers specific to prostate cancer.

Hypothesis

The hypothesis is to design a non-invasive point-of-care (POC) device for prostate cancer detection, which will have the capability to overcome the drawbacks of the conventional diagnosis and prognosis techniques.

Aims and objectives

This POC device will be fabricated by following these aims and objectives.

Aim 1: Fabrication of the nanoporous alumina samples with desired morphology by anodization.

Aim2: Functionalizing nanoporous alumina samples using 3-Aminopropyltriethoxysilane (APTES polymerization), gold nanoclusters (Au-NC), and antibody conjugation.

Aim 3: Performance assessment of the POC device in laboratory conditions.

STATE OF THE ART

What is cancer?

Cancer is a disease caused because of cells malfunctioning in our body. Cells start growing in a non-controlled way, and then they spread to other parts of the body. A mutation of the cells causes this non-controlled growth of the cells. This mutation is due to a change in the genes when cell division occurs [14]. Cancer is divided into four different stages depending on its complexity. The earliest stage is when the cancer is localized in a small area and has not spread to other tissues. In the second stage, cancer keeps growing and starts spreading to other tissues of the body near the focus of cancer. The last stage is when cancer has spread to other body organs, which refers to the metastatic phase, in which the complexity of cancer is too high, and the treatment is even more complicated. Therefore, early cancer detection is essential to provide good and highly effective treatment. To date, many tumour markers have been studied to make an early diagnosis and monitoring of cancer [15]. These markers appear at the beginning of the disease, so the study and investigation of these markers are crucial if we want to perform efficient diagnosis and treatment.

Types of cancer

The body is made from billions of cells that have different structures depending on their function in the body. For example, nerve cells and blood cells have different functions and, therefore, different structures. More than 200 types of cancers are classified based on the type of cell in which cancer starts. So, we can distinguish them into five main groups: a) carcinoma- where cancer begins in skin cells; b) sarcoma- where cancer starts in

connective tissues like bone marrow; c) then we have leukaemia, where blood cells are involved at the beginning of cancer, and finally, d) lymphoma and brain cancers. If we look at the statistics of new cancer cases diagnosed in 2021 in Spain, the most diagnosed were Bowel cancer with 43.581 cases, then prostate cancer, followed by breast cancer, and finally, lung cancer with 29.549 cases [5]. As in Spain, prostate cancer seems to be one of the major causes of cancer. Therefore, we have chosen this type of cancer for further study and propose a new technology that will help in the early diagnosis and prognosis of this type of cancer.

Prostate cancer

Prostate cancer is a type of cancer localized to men's prostate. Its origin is not clear but is related to men that consume a lot of fat, especially red meat. That is because fat stimulates and increases the production of testosterone and other hormones, which then speeds up the growth of prostate cancer, so it is also categorized as hormonal cancer. This type of cancer commonly affects men at the age of +50 years. Nowadays, the survival rate of this type of cancer is up to 95%, owing to its early diagnosis [16]. Finally, let's take a look at different cancer diagnostic techniques. The most common is the invasive one, that is, a biopsy, but there are also non-invasive methods done by analysing a urine sample, such as a prostate cancer antigen (PSA) test.

Gold Standard for sensing prostate cancer (PSA test; pros and cons)

The prostate-specific antigen (PSA) test is the gold standard for the early detection of prostate cancer. The PSA is also a protein that is produced by the prostate gland. PSA levels are measured in a PSA test by taking a blood sample from the patient's arm. Therefore, this test measures the quantity of PSA levels in capillary blood. If the results show a high level of PSA in the blood, the patient has a high probability of having prostate cancer [17]. Even PSA allows early detection of prostate cancer because of its simplicity, and it is also a widely available blood test, although it has many drawbacks. The PSA levels measured by this test can be elevated even when cancer is not present, and when the cancer is present, they can be poor. It is shown that in 85% of the cases, the results gave contradictory results, detecting up to 76% of false positives [4]. Therefore, the main drawback of the PSA test is its low reliability.

Biomarkers

In recent years, many biomarkers have been reported to replace the PSA marker because of its lack of specificity and the unnecessary biopsies done because of the use of this screening technique [18]. In this paper, we have chosen Endoglin (ENG-105) as a target biomarker, a glycoprotein shown in serum and in urine. Endoglin is shown in high levels in patients with prostate cancer, which means that this protein can be used as a potential prognostic biomarker [19]. The way to detect this type of protein is by using monoclonal antibodies (anti-ENG antibodies), which only bind with it, showing a high specificity [20].

Introduction to porous alumina, why porous alumina is important & its uses

Nanoporous alumina is a porous material obtained through the oxidation of aluminium. This oxidation is done by an electrochemical process based on an acid solution. Depending on the acid we use, we will obtain different pore sizes; for example, with sulfuric acid, we will get pores of 18-20 nm; with oxalic acid, we obtain pores sizes of 30-35 nm and finally, with phosphoric acid we obtain the larger pores +120 nm. Nanoporous alumina provides control in changing different parameters of fabrication (potential and temperature), which can then be utilized to modify the pore size range with different structures and morphologies.

So, why is alumina that important? 1) This is due to the possibility to alter the optical properties of alumina by changing the fabrication parameters, 2) it is possible to fabricate many different morphologies such as bilayers that can be used to detect more than one target [21] 3) then, due to its high effective surface area that is in the order of hundreds of m_2/cm_2, we can use this material for sensing applications [22] [23]. Apart from the sensing applications, nanoporous alumina is also

interesting for drug delivery applications [24] and tissue engineering applications, thanks to its diversity of morphologies [25] [13].

MATERIALS AND METHODS

Fabrication of nanoporous alumina

Nanoporous alumina samples were fabricated by anodizing aluminium using a two-step anodization method [26]. The anodization set-up consists of a cooler that maintains the stable temperature, the power source, and the cell samples. In this whole procedure, 0.3 M oxalic acid at 5 ºC was utilized. The method consists of first anodization lasting 20 hours at 40 V, where the pores start growing. After the first anodization, we obtained a thick aluminium oxide layer with disordered pores. The next step is to remove all the alumina from the surface by etching with chromic acid at 70 ºC for 3 hours. This step aims to obtain the aluminium surface with tiny holes from which the pores will grow in an ordered way.

Once this intermediate step is done, the samples are exposed to second anodization, which utilizes the same acid and voltage conditions as the first anodization. Additionally, sample thickness is controlled by varying the charge. In our case, we wanted 6 µm of pore length, so we applied a total of 95 C for four samples anodized simultaneously. The anodization finishes when the total charge has been applied to the samples. In our experiments, the sum of the sizes for antibody and protein is higher than 40 nm, whereas the pore size of our membranes is 35 nm. Therefore, we employed an extra step called pore widening, using phosphoric acid 5 % at 35 ºC. In this temperature condition, the growth of the pores is expected to be 1-1.5 nm/s, so we apply a pore widening reaction for 20 minutes to obtain pores up to 65 nm.

3-Aminopropyltriethoxysilane (APTES) functionalization

The surface of the NAA was functionalized by APTES, which consists of the cross-linking of amino groups on the alumina surface. This functionalization generates amino groups facilitating the immobilization of different biomolecules making the sensor selective [27]. The first step in APTES functionalization is the hydroxylation of the surface, where the samples are immersed in boiling hydrogen peroxide (H_2O_2) for 30 minutes. After the hydroxylation, the samples are stored for 1h at 60 ºC in the oven to ensure that the hydroxyl groups have attached to the NAA surface. Finally, the samples are exposed to 9.5 mL of toluene and 0.5 mL of 5% APTES. This last step aims to attach silane and amine groups to the hydroxylated alumina surface. Once the step is done, we keep the samples for 1h at 100 ºC to promote the silane cross-linking.

Surface activation and gold nanoclusters binding

The surface activation is done using 1-ethyl-3-(3-dimethyl aminopropyl)carbodiimide (EDC) and N-hydroxysuccinimide (NHS). The NHS/EDC solution is prepared in a 1:1 ratio of 6 mg of EDC and 10 mg of NHS and mixed with 2 nm gold nanoclusters solution (previously synthesized). The NHS/EDC reaction activates the carboxyl groups of the gold nanoclusters to bind them to amine-functionalized surfaces. We added 500 µL of the activated gold nanoclusters to the amine-functionalized NAA surface for 1 hour, followed by washing with deionized water (Figure 1).

Figure 1: Samples with the Au-nanoclusters solution on their surface.

Antibody functionalization

In our experiments, we have used two antibodies to test our sensors: the anti- ENG-ab, specific to the selected biomarker (Endoglin), and a control antibody (Cotinine 3), which should not bind with the protein. The gold-coated surfaces are then incubated in antibody solution (5.39 µM) for 1 hour under gentle shaking. After an hour of incubation, the functionalized surfaces were blocked using two different blocking buffers (Ethanolamine and

bovine serum albumin) for 30 min under gentle shaking to prevent the non-specific binding of proteins to the surface [28]. The samples were then washed thrice with PBS and dried with N_2 gas.

Field Emission scanning electron microscope (FESEM) characterization

FESEM was performed to analyse the pore size of the samples after the second anodization and before the pore widening reaction to analyse the real thickness of the sample. Figure 2b shows the ESEM image of NAA after the second anodization. Figure 2a shows pore growth after 20 minutes of pore widening.

Finally, figure 3 shows the cross-section of a sample anodized at 95 C (6 µm thickness expected).

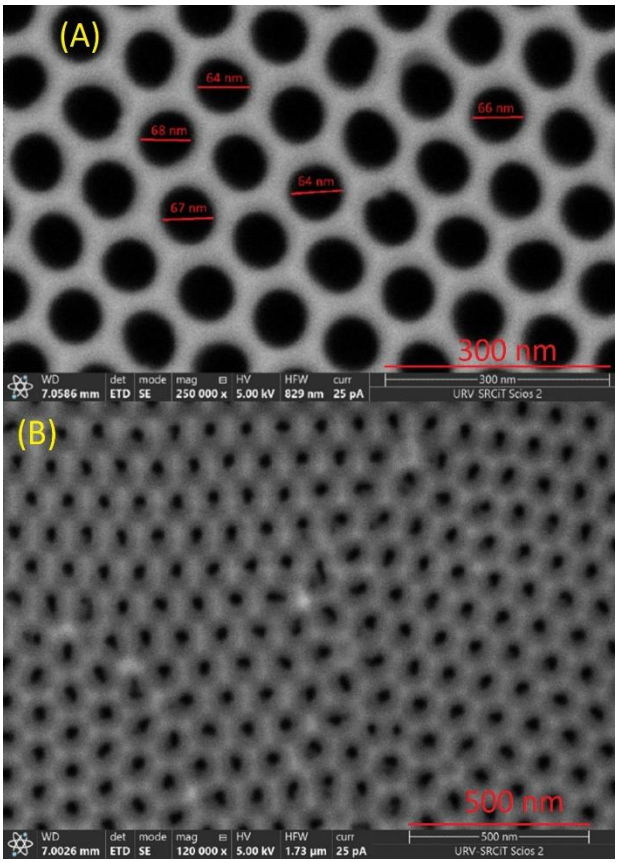

Figure 2: a) NAA sample after 20 minutes of pore widening reaction, b) NAA sample before the pore widening and after the second anodization.

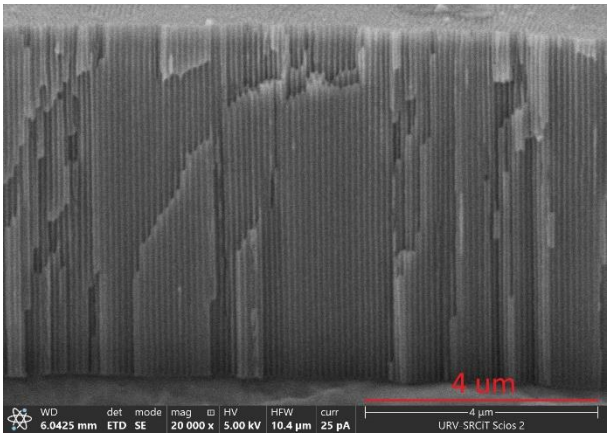

Figure 3: Cross-section of a 6 µm NAA sample obtained by anodizing the NAA at 95 C.

FTIR characterization

Fourier-transform infrared spectroscopy (FTIR) was carried out to characterize the transmittance spectra of the NAA. The NAA peak is expected to be around 1400 cm^{-1}, as seen in figure 4 in all three stages of functionalization. After hydroxylation, a wide peak at 3300 cm^{-1} was observed, corresponding to the -OH groups generated from hydrogen peroxide used in the hydroxylation step. Once the APTES functionalization was done, two peaks were observed at 2854 cm^{-1} and 2925 cm^{-1}, corresponding to the $-NH_2$ groups obtained from APTES functionalization. Finally, after protein binding, the $-NH_2$ peaks almost disappear, due to gold nanoclusters binding or/and antibody-protein binding.

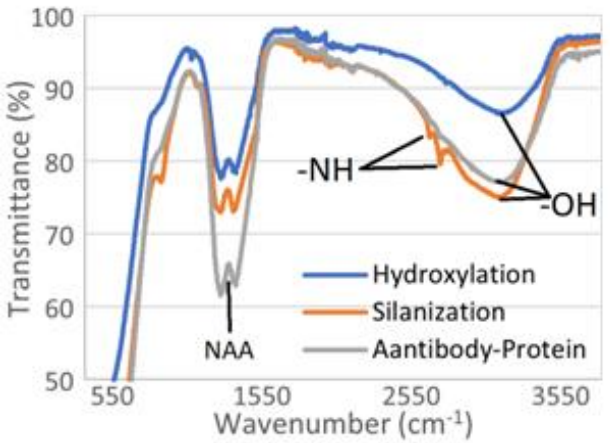

Figure 4: FTIR spectra of NAA samples in different stages of functionalization.

Reflectance characterization

The reflectance characterization was carried out with a UV-vis spectrometer. A light beam is focused on the NAA sample giving two interferences, one is reflected from the top of the pores, and the other is reflected when the light beam arrives at the bottom of the pores [29]. The overlapping of the two reflected beams generates the characteristic reflectance spectra of the NAA in the visible range (Figure 5a). These oscillations from the spectra were processed by applying the discrete Fourier transform (DFT) to get the effective optical thickness (EOT) (Figure 5b). This EOT depends on the sample's morphology (pore size and thickness) and is related to the material's refractive index, which will change depending on the morphology of the samples and on the solution that fills the pores. Therefore, the EOT value will be used as one of the sensing signals for our biosensor.

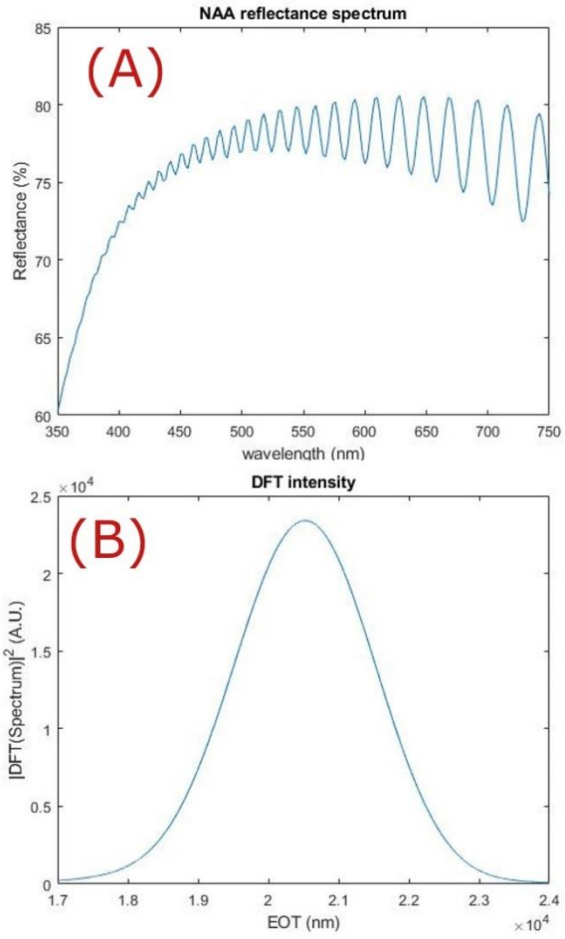

Figure 5: a) Reflectance response of NAA, b) EOT of an NAA sample after applying DFT.

Photoluminescence characterization

Photoluminescence (PL) is an optical property of a material in which the material gets excited to a higher energy state due to the absorption of light (wavelength of excitation) and emits a photon on the return of its electron back to a lower energy state [30]. A photoluminescence spectrophotometer was used to characterize gold nanoclusters modified NAA samples, which are excited with an excitation wavelength of 350 nm obtaining characteristic peaks of NAA at 450 nm and gold nanoclusters at 600 nm (Figure 6).

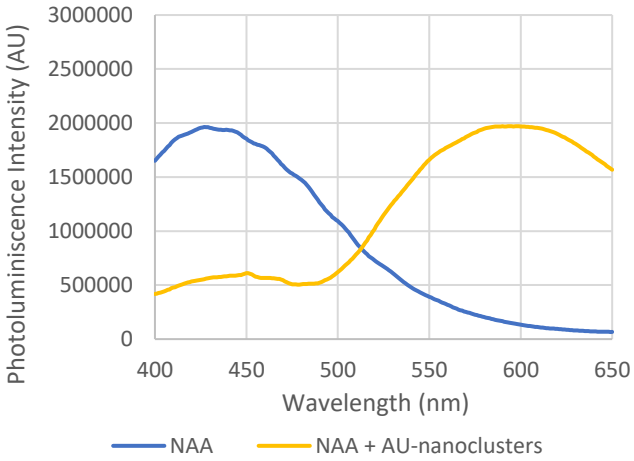

Figure 6: Photoluminescence spectra of an NAA sample and NAA + gold nanoclusters.

RESULTS AND DISCUSSION

Optimization of sensing platform (pore size, NHS/EDC coupling, and incubation time)

Four NAA samples with two different sizes (30-35 nm and 65-70 nm) were used to optimize the best pore size for gold nanoclusters binding. The gold photoluminescence signal was much more intense in the case of samples with 65-70nm pore size compared to samples with 30-35 nm pore size. Therefore, 65-70 nm pore size was used for all further experiments. Moreover, gold nanoclusters binding to APTES functionalized NAA samples were carried out using two different parameters: a) with NHS/EDC coupling and b) without NHS/EDC coupling (Figure 7). In figure 7, the grey line shows negligible photoluminescence at 600 nm from the binding of gold nanoclusters directly on APTES

functionalized NAA samples (without NHS/EDC coupling). Whereas the blue line shows better photoluminescence with NHS/EDC coupling. The photoluminescence from the two samples was measured for 2 consecutive days.

It was observed that the samples with NHS/EDC coupling were stable and had no change in photoluminescence with time (orange and blue curves). However, with time the photoluminescence from samples without NHS/EDC coupling increased significantly (yellow curve) and was comparable to those with NHS/EDC coupling. Based on these findings, we have used 65-70 nm pore size samples for all our experiments to bind gold nanoclusters without NHS/ EDC coupling.

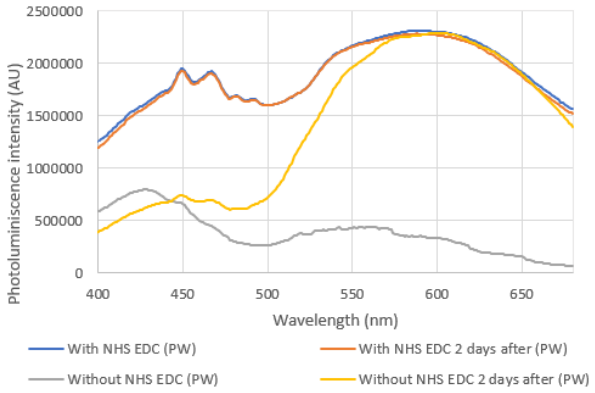

Figure 7: Photoluminescence spectra for optimizing gold nanoclusters binding on APTES modified 65-70 nm pore size NAA substrates.

Incubation time optimization

Initially, 4 NAA samples (3 sensors and 1 control) were utilized to sense 7 different concentrations (1 fg/ml, 100 fg/ml, 1 pg/ml, 100 pg/ml, 1 ng/ml, 100 ng/ml, and 1 µg/ml) of our protein of interest. Before sensing, the sensing platform was blocked by an ethanolamine blocking buffer to overcome the non-specific binding. For each sensing concentration, the modified NAA samples were incubated in the protein solution for 5 min followed by 2 min of washing in PBS under gentle shaking. Finally, the samples were dried using nitrogen gas and were then utilized to measure the effective optical thickness (EOT) and photoluminescence. Figure 8 shows a decrease in photoluminescence with an increasing concentration of proteins (anti-Eng). However, the change in photoluminescence between different concentrations was not significant. This might be either due to small incubation or washing time. Therefore, we increased the incubation time by 15 min followed by washing for 5 min in PBS. Furthermore, a minimal difference was observed (not significant) between the control and the senor. This might have occurred due to the non-specific binding of proteins. Therefore, ethanolamine and 0.1% bovine serum albumin (BSA) were utilized as blocking buffers with increased incubation and washing time.

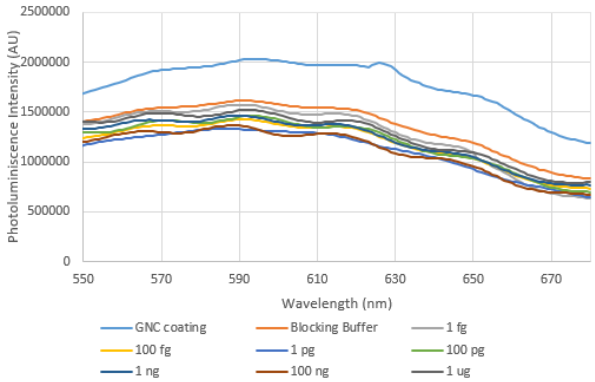

Figure 8: Changes in the Au-nanoclusters photoluminescence intensity on each endoglin concentration.

Increasing the incubation time to 15 minutes + 5 of washing in PBS using two different blocking buffers

Two sets of experiments were carried out to test our sensors. Four NAA samples (3 with the endoglin antibody and 1 with the control antibody) were prepared and tested in the first experiment. These samples were blocked using the ethanolamine blocking buffer and by increasing the incubation and the washing time to 15 minutes and 5 minutes, respectively, compared to our previous experiments. On the other hand, the second experiment consisted of 4 NAA samples. Two of these sensors were modified with the endoglin antibody, one with the control antibody and the last one without any antibody. These four samples were blocked using 0.1% bovine serum albumin (BSA) to resolve the issue underlying non-specific binding. The incubation and the washing

time were kept to 15 minutes and 5 minutes, respectively. Figure 9 shows the change in the gold photoluminescence intensity peak with a change in each concentration. This graph shows the difference between different concentrations, which can be an effect of increased incubation and washing time. The graph was similar in the case of both blocking buffers (Ethanolamine and BSA).

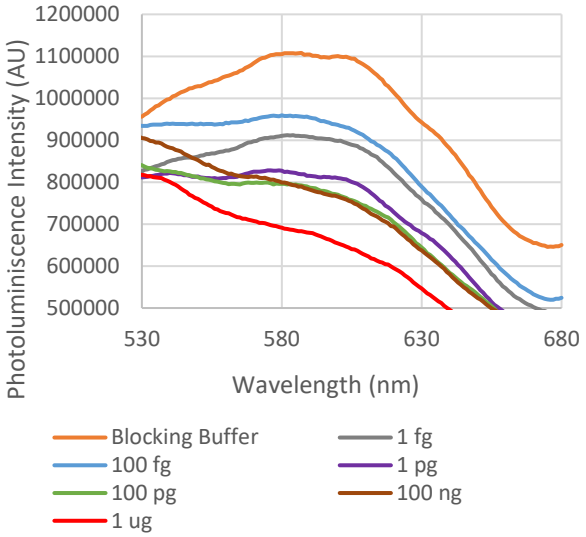

Figure 9: Photoluminescence response of the sensor while adding different endoglin concentrations.

We tested 6 sensors and 3 controls (from ethanolamine and BSA) to obtain the final graph between the sensor and the control (Figure 10). This graph shows the mean of the normalized photoluminescence intensity at various concentrations (normalized to the first concentration of 1 fg/ml). The intensity of the photoluminescence peak in the sensor decreased with an increase in the concentration from 1fg/ml to 1 ug/ml. However, a similar trend was observed in the case of our control samples, with only a minor difference from our sensor samples. This could be an effect of the blocking buffer. Therefore, our future experiments will involve the use of a blocking buffer with increased concentration or exploring a different type of blocking buffer.

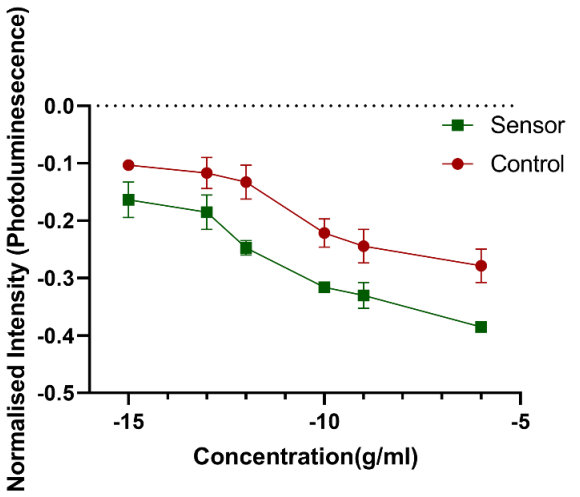

Figure 10: Normalised photoluminescence intensity changes comparison between the sensor (green line) and control sensor (red line).

Finally, we performed parallel experiments with the same sensor and control samples to evaluate the changes in the effective optical thickness (EOT) (Figure 11). We observed that the EOT decreased with an increase in the endoglin concentration. Figure 12 shows the normalized spectra of the EOT for both the control and the sensor samples (normalized to 1 fg/ml). The EOT graph behaves similarly to the photoluminescence graph (Figure 10). The graph shows that the EOT decreases with an increase in endoglin concentration in the case of our sensor. However, EOT seems to have no change or a minor increase in the case of the control samples. Furthermore, the control and the sensor samples did not show any significant differences, which can again be an effect of non-specific binding.

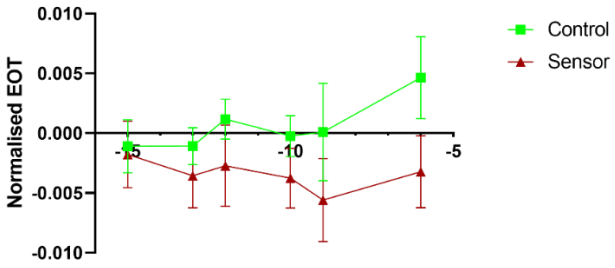

Figure 11: Normalised EOT changes comparison between the sensor (red line) and control sensor (green line).

CONCLUSION AND FUTURE WORK

In this work we used NAA samples and gold nanoclusters to detect endoglin, which is specific to prostate cancer. It has been demonstrated that the best pore size for these experiments is 65-70 nm due to the high photoluminescence intensity compared to the 30-35 nm samples. We demonstrated that irrespective of NHS+EDC coupling, the gold nanoclusters had the same photoluminescence intensity after binding to the APTES functionalized NAA sample. Moreover, the incubation time of the antigen on the sensor (15 min) compared to 5 min showed enhanced photoluminescence intensity due to improved binding of antigen to antibody. In addition, changes in EOT and photoluminescence intensity were observed on control samples demonstrating the non-specific binding on the sensor. Finally, future experiments exploiting different concentrations and types of blocking buffers should be performed to improve the specific binding of our sensor. The results presented in this thesis demonstrate a new pathway to fabricate a non-invasive POC device that can be used for the early detection of prostate cancer.

ACKNOWLEDGMENTS

This work was supported by Ministerio de Ciencia e Innovación under Grant PDI2021-128342OB-I00, grant IJC-2019-042374-1, and the Agency for Management of University and Research Grants (AGAUR) under ref. 2017-SGR-1527 and Juan de la Cierva incorporation. I also want to acknowledge Lluís Marsal and Akash Bachhuka for all the advice and guidance throughout the master's thesis.

REFERENCES

[1]. Pandya R, Grace San Diego K, Shabbir T, Modi A, Wang J, Dhahbi J et al. The cell of cancer origin provides the most reliable roadmap to its diagnosis, prognosis (biology) and therapy. Medical Hypotheses. 2021.

[2]. Plutynski A. How is cancer complex?. European Journal for Philosophy of Science. 2021.

[3]. Howlader N, Noone AM, Krapcho M, et al. (eds). SEER Cancer Statistics Review, 1975–2018. National Cancer Institute, posted to the SEER website, April 2021. Last accessed April 19, 2021.

[4]. Williams R, Lee C, Heller D. A Fluorescent Carbon Nanotube Sensor Detects the Metastatic Prostate Cancer Biomarker uPA. ACS Sensors. 2018;3(9):1838-1845.

[5]. Cancer: new cases diagnosed by type Spain 2021 | Statista [Internet]. Statista. 2022. Available from: https://www.statista.com/statistics/779054/number-from-new-cases-from-cancer-by-kind-in-spain/#professional

[6]. Mir M, Shah M, Ganai P. Nanoporous anodic alumina (NAA) prepared in different electrolytes with different pore sizes for humidity sensing. Journal of Solid State Electrochemistry. 2020;24(7):1679-1686.

[7]. Choudhari K, Choi C, Chidangil S, George S. Recent Progress in the Fabrication and Optical Properties of Nanoporous Anodic Alumina. Nanomaterials. 2022;12(3):444.

[8]. Santos A, Balderrama V, Alba M, Formentín P, Ferré-Borrull J, Pallarès J et al. Nanoporous Anodic Alumina Barcodes: Toward Smart Optical Biosensors. Advanced Materials. 2012;24(8):1050-1054.

[9]. Amouzadeh Tabrizi M, Ferré-Borrull J, Marsal L.F. Remote sensing of Salmonella-specific DNA fragment by using nanoporous alumina modified with the single-strand DNA probe. Sensors and Actuators B: Chemical. 2020;304:127302.

[10]. Garrido-Cano I, Pla L, Santiago-Felipe S, Simón S, Ortega B, Bermejo B et al. Nanoporous Anodic Alumina-Based Sensor for miR-99a-5p Detection as an Effective Early Breast Cancer Diagnostic Tool. ACS Sensors. 2021;6(3):1022-1029.

[11]. Davoodi E, Zhianmanesh M, Montazerian H, Milani A, Hoorfar M. Nano-porous anodic alumina: fundamentals and applications in tissue engineering. Journal of Materials Science: Materials in Medicine. 2020;31(7).

[12]. Jani A, Yazid H, Habiballah A, Mahmud A, Losic D. Soft and Hard Surface Manipulation of Nanoporous Anodic Aluminum Oxide (AAO). Nanoporous Alumina. 2015;:155-184.

[13]. Ferré-Borrull J., Xifré-Pérez E., Pallarès J., Marsal L.F. Optical Properties of Nanoporous Anodic Alumina and Derived Applications, Nanoporous Alumina. Springer Series in Materials Science, vol 219, pages 185-217, Losic, D., Santos, A. (eds) Springer.

[14]. Paduch R. Theories of cancer origin. European Journal of Cancer Prevention. 2015;24(1):57-67.

[15]. Schiffman J, Fisher P, Gibbs P. Early Detection of Cancer: Past, Present, and Future. American Society of Clinical Oncology Educational Book. 2015;(35):57-65.

[16]. Davis E, Beebe-Dimmer J, Yee C, Cooney K. Risk of second primary tumours in men diagnosed with prostate cancer: A population-based cohort study. Cancer. 2014;120(17):2735-2741.

[17]. Meyer A, Gorin M. First point-of-care PSA test for prostate cancer detection. Nature Reviews Urology. 2019;16(6):331-332.

[18]. Duffy M. Biomarkers for prostate cancer: prostate-specific antigen and beyond. Clinical Chemistry and Laboratory Medicine (CCLM). 2019;58(3):326-339.

[19]. Fujita K, Nonomura N. Urinary biomarkers of prostate cancer. International Journal of Urology. 2018;25(9):770-779.

[20]. González Muñoz T, Amaral A, Puerto-Camacho P, Peinado H, de Álava E. Endoglin in the Spotlight to Treat Cancer. International Journal of Molecular Sciences. 2021;22(6):3186.

[21]. Santos A, Vojkuvka L, Alba M, Balderrama V, Ferré-Borrull J, Pallarès J, Marsal L.F. Understanding and morphology control of pore modulations in nanoporous anodic alumina by discontinuous anodization. physica status solidi (a). 2012;209(10):2045-2048.

[22]. Domagalski J, Xifre-Perez E, Marsal L.F. Recent Advances in Nanoporous Anodic Alumina: Principles, Engineering, and Applications. Nanomaterials. 2021;11(2):430.

[23]. Santos A, Balderrama V, Alba M, Formentín P, Ferré-Borrull J, Pallarès J, Marsal L.F. Nanoporous Anodic Alumina Barcodes: Toward Smart Optical Biosensors. Advanced Materials. 2012;24(8):1050-1054.

[24]. Davoodi E, Zhianmanesh M, Montazerian H, Milani A, Hoorfar M. Nano-porous anodic alumina: fundamentals and applications in tissue engineering. Journal of Materials Science: Materials in Medicine. 2020;31(7).

[25]. Jani A, Yazid H, Habiballah A, Mahmud A, Losic D. Soft and Hard Surface Manipulation of Nanoporous Anodic Aluminum Oxide (AAO). Nanoporous Alumina. 2015;:155-184.

[26]. Santos A, Ferré-Borrull J, Pallarès J, Marsal L.F. Hierarchical nanoporous anodic alumina templates by asymmetric two-step anodization. physica status solidi (a). 2010;208(3):668-674.

[27]. Hsiao V, Waldeisen J, Zheng Y, Lloyd P, Bunning T, Huang T. Aminopropyltriethoxysilane (APTES)-functionalized nanoporous polymeric gratings: fabrication and application in biosensing. Journal of Materials Chemistry. 2007;17(46):4896.

[28]. Yang P, Mahmood T. Western blot: Technique, theory, and trouble shooting. North American Journal of Medical Sciences. 2012;4(9):429.

[29]. Pol L, Acosta L, Ferré-Borrull J, Marsal L.F. Aptamer-Based Nanoporous Anodic Alumina Interferometric Biosensor for Real-Time Thrombin Detection. Sensors. 2019;19(20):4543.

[30]. Gasenkova I, Mukhurov N, Zhvavyi S, Kolesnik E, Stupak A. Photoluminescent properties of nanoporous anodic alumina doped with manganese ions. Journal of Luminescence. 2017;185:298-305.

Josep Maria Cantons Pérez

SUPPORTING INFORMATION

LABEL-FREE SENSOR FOR THE NEAR REAL-TIME DETECTION OF PROSTATE CANCER

MASTER'S DEGREE THESIS

Supervised by Dr. Lluis F. Marsal and Dr. Akash Bachhuka

MASTER'S DEGREE IN NANOSCIENCE, MATERIALS AND PROCESSES

UNIVERSITAT ROVIRA I VIRGILI

Tarragona

2022

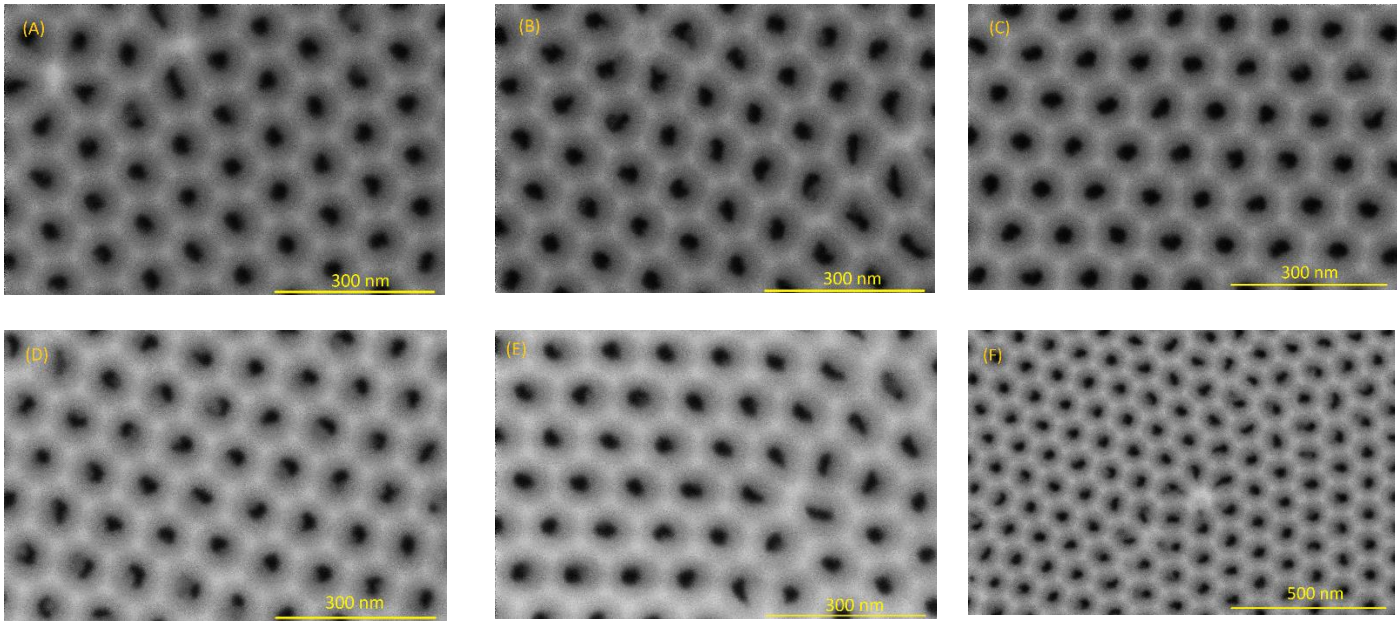

Figure S1: Top view FESEM images of NAA samples after second anodization. A) 29 nm average pore size, b) 33 nm average pore size, c) 30 nm average pore size, d) 31 nm average pore size, e) 33 nm average pore size and f) 32 nm average pore size. In these images it is shown that after the two-two step anodization with oxalic acid at 5 ºC and 40 V we obtain pore sizes from 30 nm to 35 nm.

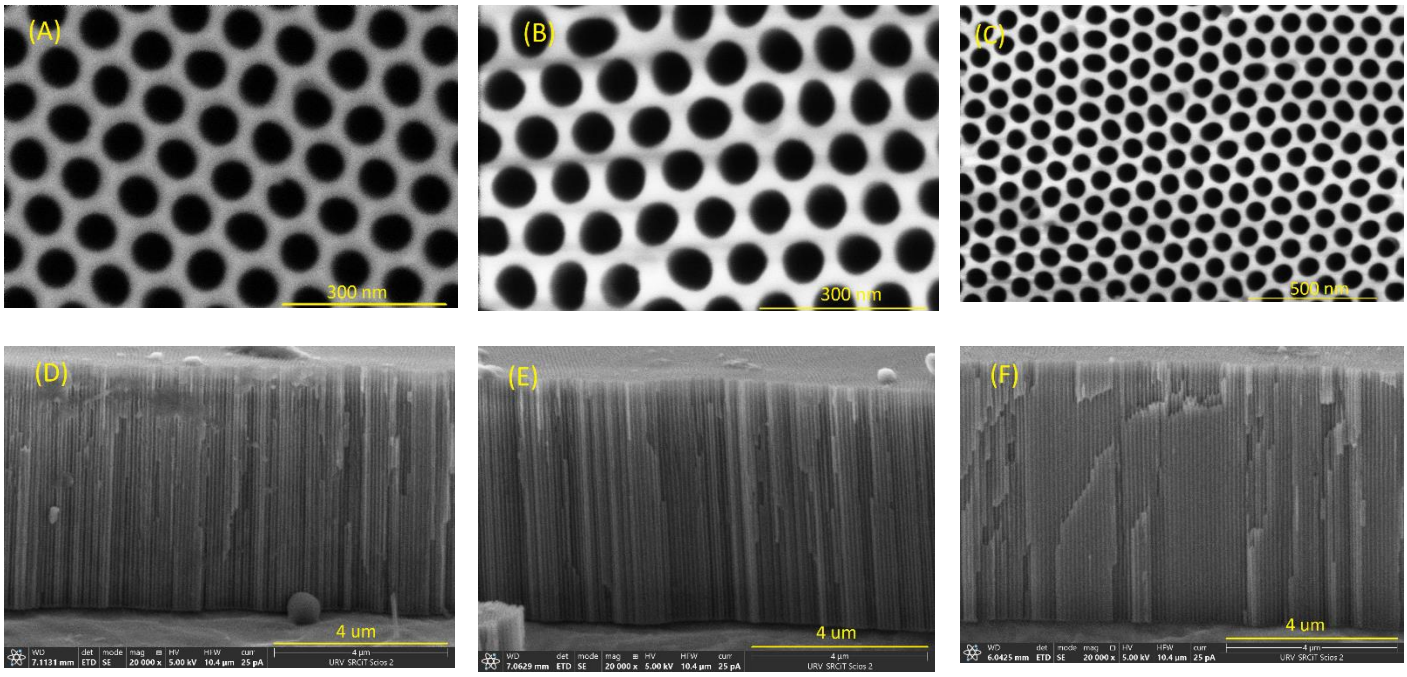

Figure S2: Top view of NAA samples after 22 minutes of pore widening and cross section of NAA samples after a second anodization (95 C). A) 65 nm average pore size, b) 69 nm average pore size, c) 69 nm average pore size, d) 5.7 µm average thickness, e) 5.8 µm average thickness and f) 6.1 µm average thickness. The first three images show that after 22 minutes of pore widening, we can obtain pore sizes higher than 65 nm, and the three below show that after applying 95 C on the second anodization we obtain approximately 6 µm of pore length.

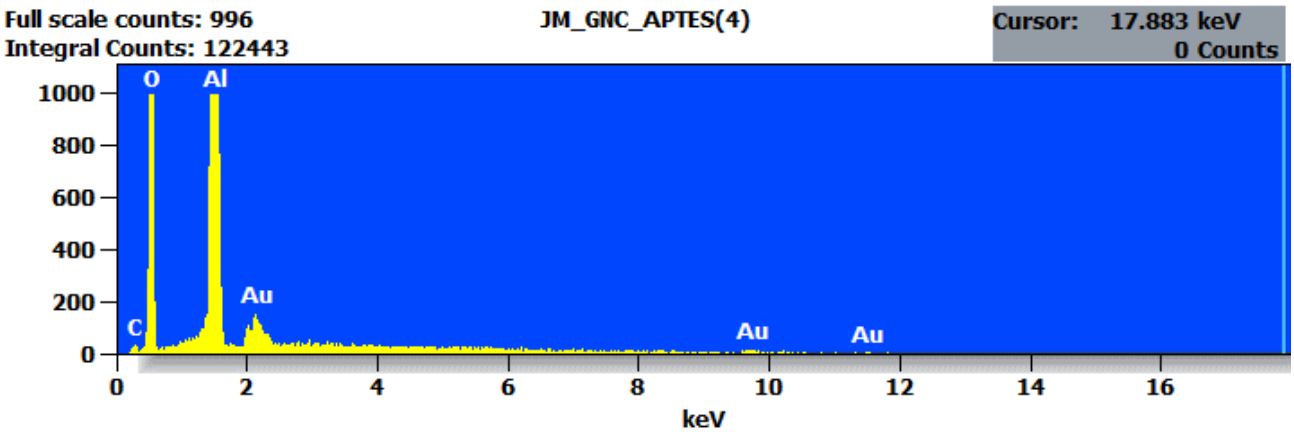

Element	Weight %	Weight % Error	Norm. Wt.%	Atom %
C	1.35	± 0.11	1.35	2.43
O	39.45	± 0.33	39.45	53.19
Al	54.91	± 0.26	54.91	43.91
Au	4.29	± 0.82	4.29	0.47
Total	100.00		100.00	100.00

Figure S3: EDX spectra obtained through the FESEM, of a NAA sample functionalized with gold nanoclusters. The image shows the two intensities that corresponds to the Au, and in the table the molecular weight that is present on the sample.

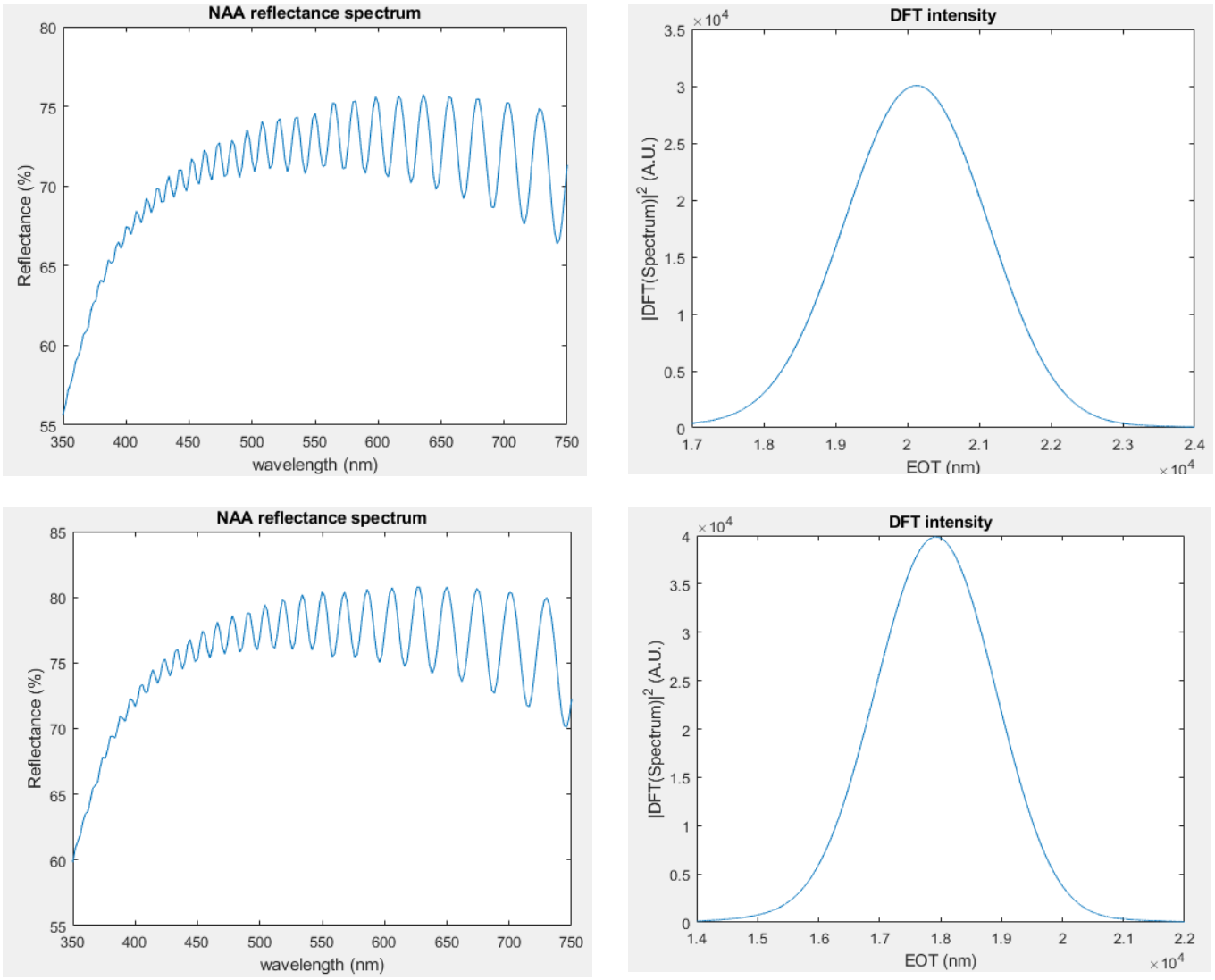

Figure S4: Reflectance spectrums of NAA samples and their respective effective optical thickness calculation through the discreet Fourier transform (DFT). On the top images it is shown the reflectance spectra of a sample after a second anodization (30 -35 nm pore size) having on right side the effective optical thickness value. On the bottom we have the reflectance spectra of NAA samples after 20 minutes of pore widening, having on right side the effective optical thickness value. We can see that the spectra of the sample with bigger pore sizes (bottom images) the EOT has decrease due to the increment of the pore size in the sample.

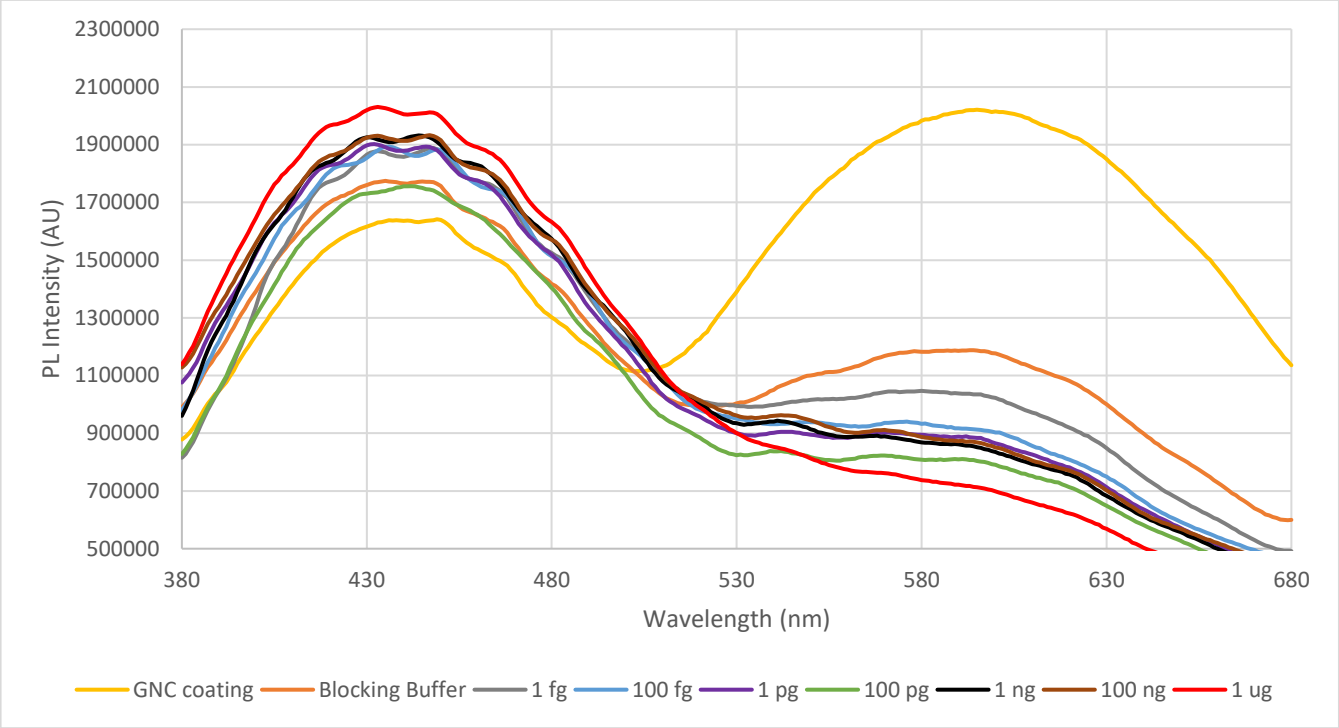

Figure S5: Photoluminescence spectra of the control (using the control antibody). The figure shows the changes in PL intensity while applying the different concentrations of the Endoglin, first experiments with 5 minutes of incubation time. It shows that the PL intensity is decreasing but without any patron as it is a control.

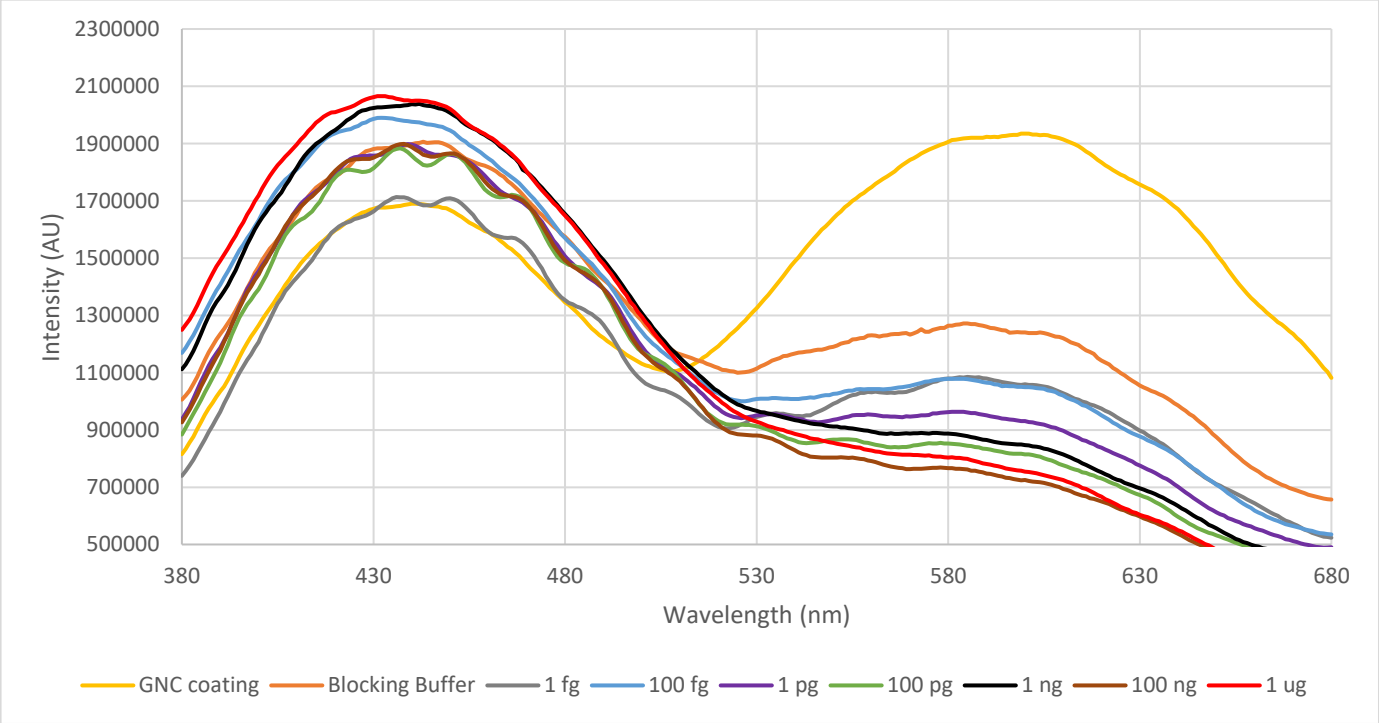

Figure S6: Photoluminescence spectra of one of the sensors. This one shows the changes in the PL intensity while we add different concentrations of endoglin, this time the conditions of the incubation time are also 5 minutes. It shows better changes compared with the control sensor (Figure S5), but still not sufficient for the final sensor due to the need of further optimization.